Article

Does the Solid–Liquid Crystal Phase Transition Provoke the Spin-State Change in Spin-Crossover Metallomesogens?

M. Seredyuk, A. B. Gaspar, V. Ksenofontov, Y. Galyametdinov, J. Kusz, and P. Gtlich

J. Am. Chem. Soc., **2008**, 130 (4), 1431-1439 • DOI: 10.1021/ja077265z

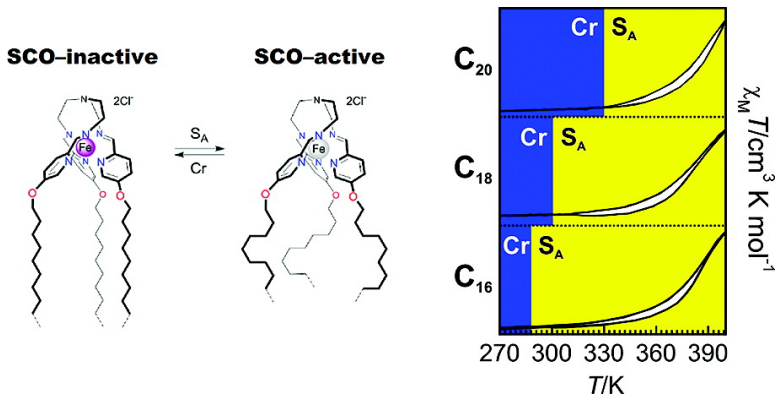

More About This Article

Additional resources and features associated with this article are available within the HTML version:

- Supporting Information
- Links to the 4 articles that cite this article, as of the time of this article download
- Access to high resolution figures
- Links to articles and content related to this article
- Copyright permission to reproduce figures and/or text from this article

View the Full Text HTML

J|A|C|S
ARTICLES
Published on Web 01/09/2008

Does the Solid−Liquid Crystal Phase Transition Provoke the Spin-State Change in Spin-Crossover Metallomesogens?

M. Seredyuk,[†] A. B. Gaspar,*[,‡] V. Ksenofontov,[†] Y. Galyametdinov,[§] J. Kusz,[||] and P. Gütlich*[,†]

Institut für Anorganische und Analystiche Chemie, Johannes-Gutenberg-Universität, Staudinger-Weg 9, D-55099 Mainz, Germany, Institut de Ciència Molecular/Departament de Química Inorgànica, Universitat de València, Edifici de Instituts de Paterna, Apartat de Correus 22085, E-46071 València, Spain, Kazan Physical Technical Institute, Russian Academy of Science, Sibirsky Tract 10/7, 420029, Kazan, Russia, and Institute of Physics, University of Silesia, 4 Uniwersytecka Street, 40007 Katowice, Poland

Received September 19, 2007

Abstract: Three types of interplay/synergy between spin-crossover (SCO) and liquid crystalline (LC) phase transitions can be predicted: (i) systems with coupled phase transitions, where the structural changes associated to the Cr↔LC phase transition drives the spin-state transition, (ii) systems where both transitions coexist in the same temperature region but are not coupled, and (iii) systems with uncoupled phase transitions. Here we present a new family of Fe(II) metallomesogens based on the ligand tris[3-aza-4-((5-C_n)(6-R)(2-pyridyl))but-3-enyl]amine, with C_n = hexyloxy, dodecyloxy, hexadecyloxy, octadecyloxy, eicosyloxy, R = hydrogen or methyl (C_n-trenH or C_n-trenMe), which affords examples of systems of types i, ii, and iii. Self-assembly of the ligands C_n-trenH and C_n-trenMe with $Fe(A)_2 \cdot xH_2O$ salts have afforded a family of complexes with general formula $[Fe(C_n\text{-trenR})](A)_2 \cdot sH_2O$ ($s \geq 0$), with A = ClO_4^-, F^-, Cl^-, Br^- and I^-. Single-crystal X-ray diffraction measurements have been performed on two derivatives of this family, named as $[Fe(C_6\text{-trenH})](ClO_4)_2$ (C_6-**1**) and $[Fe(C_6\text{-trenMe})](ClO_4)_2$ (C_6-**2**), at 150 K for C_6-**1** and at 90 and 298 K for C_6-**2**. At 150 K, C_6-**1** displays the triclinic space group $P\bar{1}$, whereas at 90 and at 298 K C_6-**2** adopts the monoclinic $P2_1/c$ space group. In both compounds the iron atoms adopt a pseudo-octahedral symmetry and are surrounded by six nitrogen atoms belonging to imino groups and pyridines of the ligands C_n-trenH and C_n-trenMe. The average Fe(II)−N bonds (1.963(2) Å) at 150 K denote that C_6-**1** is in the low-spin (LS) state. For C_6-**2** the average Fe(II)−N bonds (2.007(1) Å) at 90 K are characteristic of the LS state, while at 298 K they are typical for the high-spin (HS) state (2.234(3) Å). Compound C_6-**1** and $[Fe(C_{18}\text{-trenH})](ClO_4)_2$ (C_{18}-**1**) adopts the LS state in the temperature region between 10 and 400 K, while compound C_6-**2** and $[Fe(C_n\text{-trenMe})](ClO_4)_2$ (n = 12 (C_{12}-**2**), 18 (C_{18}-**2**)) exhibit spin crossover behavior at $T_{1/2}$ centered around 140 K. The thermal spin transition is accompanied by a pronounced change of color from dark red (LS) to orange (HS). The light-induced excited spin state trapping (LIESST) effect has been investigated in compounds C_6-**2**, C_{12}-**2** and C_{18}-**2**. The $T_{1/2}^{LIESST}$ is 56 K (C_6-**2**), 48 K (C_{16}-**2**), and 56 K (C_{18}-**2**). On the basis of differential scanning calorimetry, optical polarizing microscopy, and X-ray diffraction findings for C_{18}-**1**, C_{12}-**2**, and C_{18}-**2** at high temperature a smectic mesophase S_X has been identified with layered structures similar to C_6-**1** and C_6-**2**. The compounds $[Fe(C_n\text{-trenH})](Cl)_2 \cdot sH_2O$ (n = 16 (C_{16}-**3**, s = 3.5, C_{16}-**4**, s = 0.5, C_{16}-**5**, s = 0), 18 (C_{18}-**3**, s = 3.5, C_{18}-**4**, s = 0.5, C_{18}-**5**, s = 0), 20 (C_{20}-**3**, s = 3.5, C_{20}-**4**, s = 0.5, C_{20}-**5**, s = 0)) and $[Fe(C_{18}\text{-tren})](F)_2 \cdot sH_2O$ (C_{18}-**6**, s = 3.5, C_{18}-**7**, s = 0) show a very particular spin-state change, while $[Fe(C_{18}\text{-tren})](Br)_2 \cdot 3H_2O$ (C_{18}-**8**) together with $[Fe(C_{18}\text{-tren})](I)_2$ (C_{18}-**9**) are in the LS state (10−400 K) and present mesomorphic behavior like that observed for the complexes C_{18}-**1**, C_{12}-**2**, and C_{18}-**2**. In compounds C_n-**3** 50% of the Fe(II) ions undergo spin-state change at $T_{1/2}$ = 375 K induced by releasing water, and in partially dehydrated compounds (s = 0.5) the Cr→S_A phase transition occurs at 287 K (C_{16}-**4**), 301 K (C_{18}-**4**) and 330 K (C_{20}-**4**). For the fully dehydrated materials C_n-**5** 50% of the Fe(II) ions are in the HS state and show paramagnetic behavior between 10 and 400 K. In the partially dehydrated C_n-**4** the spin transition is induced by the change of the aggregate state of matter (solid↔liquid crystal). For compound C_{18}-**6** the full dehydration to C_{18}-**7** provokes the spin-state change of nearly 50% of the Fe(II) ions. The compounds C_n-**3** and C_{18}-**6** are dark purple in the LS state and become light purple−brown when 50% of the Fe(II) atoms are in the HS state.

Introduction

The interest in the tailoring of multifunctional materials combining spin-crossover (SCO)[1] and liquid crystalline (LC)[2] behavior arises from the potential properties derived from the presence of metal ions within anisotropic phases.[3] These kinds of materials are new examples of functional metallomesogens,[4] a recently developed type of mesogenic materials. The so-called SCO phenomenon is observed in transition-metal ions with $3d^n$ (n = 4−7) electronic configurations. The vast majority of SCO

[†] Johannes-Gutenberg-Universität.
[‡] Universitat de València.
[§] Russian Academy of Science.
[||] University of Silesia.

(1) (a) Gütlich, P., Goodwin, H. A., Eds. Spin Crossover in Transition Metal Compounds. *Topics in Current Chemistry;* Springer: Berlin, 2004; Vol. 233, 234, 235. (b) Gaspar, A. B.; Ksenofontov, V.; Seredyuk, M.; Gütlich, P. *Coord. Chem. Rev.* **2005**, *249*, 2661−2676. (c) Real, J. A.; Gaspar, A. B.; Muñoz, M. C. *Dalton Trans.* **2005**, 2062−2079. (d) Real, J. A.; Gaspar, A. B.; Niel, V.; Muñoz, M. C.; *Coord. Chem. Rev.* **2003**, *236*, 121−141. (e) Gütlich, P.; Hauser, A.; Spiering, H. *Angew. Chem., Int. Ed. Engl.* **1994**, *33*, 2024−2054. (f) Gütlich, P.; Garcia, Y. *Top. Curr. Chem.* **2004**, *234*, 49−62.

compounds reported so far concerns Fe(II) and Fe(III) complexes, to a lesser extent Co(II), and only in a few cases Mn(III) and Cr(II) complexes.[1f] SCO materials display labile electronic configurations switchable between the high-spin (HS) and low-spin (LS) states leading to distinctive changes in magnetism, color and structure, which may be driven by variation of temperature and/or pressure[1] and by light irradiation (light-induced excited spin state trapping (LIESST) effect).[5] Their magnetic, optical and structural properties may be altered drastically in a narrow range of temperature and/or pressure for cooperative spin transitions. Cooperativity may be accompanied by hysteresis (memory effect) when the cohesive forces, communicating between the SCO centers in the solid state, propagate the structural changes cooperatively throughout the whole lattice. A crossover between the HS and LS configurations occurs when the change of the Gibbs free energy $\Delta G_{HL} = G_{HS} - G_{LS}$ is in the range of thermal energy.[1]

A single material combining spin crossover and liquid crystalline behavior may lead to a number of advantages in practical applications, for example, processing spin crossover materials in the form of thin films, enhancement of spin transition signals, switching and sensing in different temperature regimes, or achievement of photo- and thermochromism in metal-containing liquid crystals.[1b−c,4a] The change of color is certainly a phenomenon which is of interest in the field of liquid crystals. The interest lies in the necessity for color in a number of applications in liquid crystals such as passive blocking filters, laser addressed devices, polarizers based on dichroic effects, or the utility of thermochromism.[4] While color change has rarely been observed for nonchiral organic liquid crystals,[6] several papers have reported thermochromism in nonchiral metal-containing liquid crystals.[7] More successful has been the development of cholesteric liquid crystals[8] for the production of colored electro-optical films together with the liquid crystal OLEDs.[9] Worth mentioning is also the achievement of photochromic organic liquid crystals.[10]

A first step aiming to achieve a material gathering SCO and LC properties has led to an iron(III) metallomesogen where both properties are not synchronous but they appear in different temperature intervals.[11] Hayami and co-workers[12] have also reported mononuclear iron(II) complexes in which the spin transition and the smectic mesophases appear at different temperature intervals. Recently, we have investigated the possibility to synchronize both transitions, spin transition and solid−liquid crystal transition, in Fe(II) complexes.[13] The first step in the tailoring of these multifunctional materials has been the choice of SCO systems showing abrupt spin transition near or above room temperature. This is the range of temperatures at which usually the LC phase transition is observed. In this respect, the polymeric SCO compounds based on the triazole-based ligands are among the best candidates, showing abrupt spin transition above or near to room temperature accompanied by a pronounced change of color.[1] The second step in this approach has concerned the incorporation of the LC moiety into the SCO system, which implies the attachment of the aromatic core with the alkyl chains to the triazole ligand. In the synthesized Fe(II) metallomesogens, $[Fe(C_n\text{-trz})_3](4\text{-}MeC_6H_4\text{-}SO_3)_2 \cdot xH_2O$,[13] SCO occurs in the room-temperature range where the materials show a discotic columnar mesophase D_{hd}. The change of the spin state is accompanied by a pronounced change of color from purple (LS state) to white (HS state). We have provided experimental evidence that $[Fe(C_n\text{-trz})_3](4\text{-}MeC_6H_4\text{-}SO_3)_2$ metallomesogens present discotic columnar mesophase in the temperature interval of 200−475 K where the thermal spin transition occurs. Realization of the crystalline state of these materials is difficult, in fact, no melting point has been observed.[13] Therefore, we concluded, in contrast to previous work,[14] that the spin-transition behavior in these metallomesogens is not driven by a phase transition from the crystalline state to the liquid crystal state. On the other hand, spin-state transition induced by mechanical strength on going to the amphiphilic mesophase in metallo-supramolecular polyelectrolytes organized in LB films has been proposed, however, not yet experimentally demonstrated.[15] Presently, the number of reported SCO metallomesogens is rather scarce, and the spin-transition phenomena in these materials was found to be governed by the classical factors which are well-known to affect the SCO and its characteristics (*T*c, hysteresis), namely, subtle structural and electronic modifications tuned by the crystal packing, which determines the ligand field strength and the SCO behavior. These modifications depend essentially on the nature of the ligands, the non-coordinating anions, the solvent molecules, and the crystal packing. Complete control of these variables is a rather difficult task to accomplish.

The question is actually posed as whether the change of aggregate of the matter (solid−liquid crystal) drives the spin-

(2) (a) Laschat, S.; Baro, A.; Steinke, N.; Giesselmann, F.; Hägele, C.; Scalia, G.; Judele, R.; Kapatsina, E.; Sauer, S.; Schreivogel, A.; Tosoni, M. *Angew. Chem., Int. Ed.* **2007**, *46*, 4832−4887 and references therein. (b) Donnio, B.; Guillon, D. *Adv. Polym. Sci.* **2006**, *201*, 45−155. (c) Camerel, F.; Donnio, B.; Bourgogne, C.; Schmutz, M.; Guillon, D.; Davidson, P.; Ziessel, R. *Chem. Eur. J.* **2006**, *16*, 4261−4274. (d) Reddy, R. A.; Tschierske, C. *J. Mater. Chem.* **2006**, *10*, 907−961. (e) Binnemans, K. *Chem. Rev.* **2005**, *11*, 4148−4204. (f) Paleos, C. M.; Tsiourvas, D. *Angew. Chem., Int. Ed.* **1995**, *16*, 1696−1711.

(3) Rowan, S. J. *Angew. Chem., Int. Ed.* **2005**, *44*, 4830−4832.

(4) (a) Serrano, J. L. *Metallomesogens;* VCH: Weinheim, Germany, 1996 and references therein. (b) Hudson, S. A.; Maitlis, P. M. *Chem. Rev.* **1993**, *93*, 861. (c) Donnio, B.; Bruce, D. W. *Struct. Bond.* **1999**, *95*, 193−247. (d) Lemieux, R. P. *Acc. Chem. Res.* **2001**, *34*, 845−853. (e) Gimenez, R.; Lydon, D. P.; Serrano, J. L. *Curr. Opin. Solid State Mater. Sci.* **2002**, *6*, 527−535. (f) Serrano, J. L.; Sierra, T. *Coord. Chem. Rev.* **2003**, *242*, 73−85. (g) Donnio, B. *Curr. Opin. Colloid, Interface Science State Mater. Sci.* **2002**, *7*, 371−394. (h) Bruce, D. W. *Acc. Chem. Res.* **2000**, *33*, 831−840. (i) Piguet, C.; Bünzli, J. C. G.; Donnio, B.; Guillon, D. *Chem. Commun.* **2006**, *36*, 3755−3768.

(5) (a) Decurtins, S.; Gütlich, P.; Köhler, C. P.; Spiering, H.; Hauser, A. *Chem. Phys. Lett.* **1984**, *105*, 1−4. (b) Lètard, J.-F. *J. Mater. Chem.* **2006**, *16*, 2550−2559.

(6) Shvartsman, F. P.; Krongauz, V. A. *Nature* (*London*) **1984**, *309*, 608−611.

(7) (a) Bruce, D. W.; Dunmur, P. A.; Esteruelas, M. A.; Hunt, S. E.; Maitlis, P. M.; Marsden, J. R.; Sola, E.; Stacey, J. M. *J. Mater. Chem.* **1991**, *1*, 251−255. (b) Ohta, K.; Hasabe, H.; Moriya, M.; Fujimoto, T.; Yamamoto, I. *J. Mater. Chem.* **1991**, *1*, 831−834. (c) Gregg, B. A.; Fox, M. A.; Bard, A. J. *J. Phys. Chem.* **1989**, *93*, 4227−4234.

(8) De Filpo, G.; Nicoletta, F. P.; Chidichimo, G. *Adv. Mater.* **2005**, *17*, 1150−1152.

(9) Aldred, M. P.; Contoret, A. E. A.; Farrar, S. R.; Stephen, M. K.; Mathieson, D.; O' Neill, M.; Tsoi, W. C.; Vlachos, P. *Adv. Mater.* **2005**, *17*, 1368−1372.

(10) (a) Frogoli, M.; Mehl, G. H. *Chem. Phys. Chem.* **2003**, *1*, 101−103. (b) Irie, M. *Chem. Rev.* **2000**, *100*, 1685.

(11) Galyametdinov, Y.; Ksenofontov, V.; Prosvirin, A.; Ovchinnikov, I.; Ivanova, G.; Gütlich, P.; Haase, W. *Angew. Chem., Int. Ed.* **2001**, *40*, 4269−4271.

(12) (a) Hayami, S.; Danjobara, K.; Inoue, K.; Ogawa, Y.; Matsumoto, N.; Maeda, Y. *Adv. Mater.* **2004**, *16*, 869−872. (b) Hayami, S.; Motokawa, N.; Shuto, A.; Masuhara, N.; Someya, T.; Ogawa, Y.; Inoue, K.; Maeda, Y. *Inorg. Chem.* **2007**, *46*, 1789−1794.

(13) Seredyuk, M.; Gaspar, A. B.; Ksenofontov, V.; Reiman, S.; Galyametdinov, Y.; Haase, W.; Rentschler, E.; Gütlich, P. *Chem. Mater.* **2006**, *18*, 2513−2519.

(14) Fujigaya, T.; Jiang, D. L.; Aida, T. *J. Am. Chem. Soc.* **2003**, *125*, 14690−14691.

(15) Bodenthin, Y.; Pietsch, U.; Möhwald, H.; Kurth, D. G. *J. Am. Chem. Soc.* **2005**, *127*, 3110−3114.

Chart 1

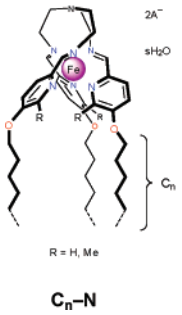

Anion A	R	Compound
ClO_4^-	H	**C_6–1**, **C_{18}–1**
	Me	**C_6–2**, **C_{12}–2**, **C_{18}–2**
Cl^-	H	**C_{16}–3** →[a] **C_{16}–4** → **C_{16}–5**
		C_{18}–3 → **C_{18}–4** → **C_{18}–5**
		C_{20}–3 → **C_{20}–4** → **C_{20}–5**
F^-	H	**C_{18}–6** → **C_{18}–7**
Br^-	H	**C_{18}–8**
I^-	H	**C_{18}–9**

[a] Arrows show relation of the compounds upon dehydration. For details, see explanation in text.

state change or only affects the cooperative process of the SCO phenomena. Three types of interplay/synergy between SCO and LC phase transitions can be predicted: (i) systems with coupled phase transitions, where the structural changes associated to the Cr↔LC phase transition drives the spin state transition, (ii) systems where both transitions coexist in the same temperature region but are not coupled, and (iii) systems with uncoupled phase transitions. Here we shall present a new family of Fe(II) metallomesogens based on the ligand tris[3-aza-4-((5-C_n)(6-R)-(2-pyridyl))but-3-enyl]amine, with C_n = hexyloxy, dodecyloxy, hexadecyloxy, octadecyloxy, eicosyloxy, R = hydrogen or methyl ($C_{6,16,18,20}$-trenH or $C_{6,12,18}$-trenMe), which affords examples of systems of types i, ii, and iii. We shall present an analysis of the factors that govern the SCO process in these materials and discuss the synergy between SCO and LC phase transitions observed in materials of type i.

Results and Discussion

Self-assembly of the ligands C_n-trenH and C_n-trenMe with $Fe(A)_2 \cdot sH_2O$ salts have afforded a family of complexes with general formula $[Fe(C_n\text{-trenR})](A)_2 \cdot sH_2O$ ($s \geq 0$), with A = ClO_4^-, F^-, Cl^-, Br^-, and I^- (Chart 1). Single-crystal X-ray diffraction measurements have been performed on two derivatives of this family of metallomesogens, named as $[Fe(C_6\text{-trenH})](ClO_4)_2$ (C_6-**1**) and $[Fe(C_6\text{-trenMe})](ClO_4)_2$ (C_6-**2**), at 150 K for C_6-**1** and at 90 and 298 K for C_6-**2**.

Crystal structure of C_6-1 and C_6-2. Figure 1a and Figure 2a,b illustrate the molecular structures of both compounds together with the corresponding atom numbering scheme. At 150 K, C_6-**1** displays the triclinic space group $P\bar{1}$, whereas at 90 and at 298 K C_6-**2** adopts the monoclinic $P2_1/c$ space group. A selection of crystallographic data and bond distances are given in the Supporting Information STable 1 and STable 2. The iron atoms adopt a pseudo-octahedral symmetry and are surrounded by six nitrogen atoms belonging to imino groups and pyridines of the trifurcated ligands C_n-trenH and C_n-trenMe. In C_6-**1** each cell contains two independent complex molecules of opposite chirality (Figure 1a). The average Fe(II)−N bonds (1.963(2) Å) and the distortion parameter Σ (67.56(8)°) at 150 K denote that C_6-**1** is in the LS state. The amphiphilic nature of the alkylated molecules results in the self-assembly into bilayered composite with one layer being made up of polar head groups together with perchlorate anions. The nonpolar chains from oppositely directed molecules meet together leading to a hydrocarbon layer. Almost fully stretched alkyl chains are only distorted by the gauche conformation of some of the methylene groups (Figure 1b) and tilted toward the *ac* plane but do not intertwine with those of adjacent layers. If compared with the unalkylated complex $\{Fe[tren(Py)_3]\}(ClO_4)_2$,[16] the introduction of alkyl chains into the complex molecule affects the crystal packing causing in C_6-**1** the segregation into a layered structure. In $\{Fe[tren(Py)_3]\}(ClO_4)_2$ the hydrogen-bonding network has a three-dimensional character, while in C_6-**1** all CH···O(Cl) contacts (2.428(2)−2.719(2) Å) belong to the two-dimensional hydrogen-bonding network formed within the ionic layers. For C_6-**2** (Figure 2a and b) the average Fe(II)−N bonds (2.007(1) Å) and the distortion parameter Σ (85.54(7)°) at 90 K are characteristic of the LS state while at 298 K they are typical for the HS state (2.234(3) Å, 116.59(11)°). Modifications of the coordination sphere of C_6-**2** due to spin transition are directly reflected in the metal-to-ligand bond length, which is illustrated by the distinguishable divergence of the overlapped HS and LS structures (Figure 2c). In the HS form the distances Fe−N(ligand) are longer, consequently, the volume of the $[FeN_6]$ chromophore increases. C_6-**2** displays similar crystal packing like observed in C_6-**1** despite both compounds crystallizing in different space groups (SFigure 6). The crystal packing in the LS and HS structures for C_6-**2** is almost identical, with CH··· O(Cl) contacts being 2.308(5)−2.781(5) Å (HS) and 2.301(5)−2.718(5) Å (LS).

Magnetic and Mesomorphic Behavior of Compounds C_n-1 (n = 6, 18) and C_n-2 (n = 6, 12, 18). Compound C_6-**1** and $[Fe(C_{18}\text{-trenH})](ClO_4)_2$($C_{18}$-**1**) adopt the LS state in the temperature region between 10 and 400 K, where the temperature dependence of the magnetic susceptibility has a constant value of 0.10 cm^3 K mol^{-1} (SFigure 2). The Mössbauer spectrum of C_6-**1** recorded at 80 K points out two nonequivalent Fe(II) atoms, both in the LS state (SFigure 3, STable 1). The Mössbauer spectrum of C_{18}-**1** recorded at 80 K, however, could be satisfactorily fitted with only one LS doublet. Introduction of the methyl group in the C_n-trenR ligand has resulted in a noticeable modification of the crystal-field strength at the iron(II) center. Compound C_6-**2** and $[Fe(C_n\text{-trenMe})](ClO_4)_2$ n = 12 (C_{12}-**2**), 18 (C_{18}-**2**) exhibit spin crossover behavior at $T_{1/2}$ centered around 140 K, the temperature at which the number of molecules in the HS and LS states is equal. Figure 3 depicts the $\chi_M T$ versus T plots for C_6-**2**, C_{12}-**2**, and C_{18}-**2** (χ_M stands for the molar magnetic susceptibility and T the temperature). The spin transition is complete and relatively continuous for C_6-**2**, C_{12}-**2**, and C_{18}-**2** with $T_{1/2}$ = 146, 120, and 133 K, respectively. Mössbauer spectra recorded below and above $T_{1/2}$ for C_6-**2**, C_{12}-**2**, and C_{18}-**2** are consistent with the magnetic and structural data reported (SFigure 3). The thermal spin transition is accompanied by a pronounced change of color from dark red (LS) to orange (HS). The LIESST effect[5] has been investigated in compounds C_6-**2**, C_{12}-**2**, and C_{18}-**2**. The LS ground state was photoconverted at 4 K to a metastable HS state after irradiation of samples with light of λ = 514 nm (25 mW cm^{-2}) (Figure 3a).[21] The highest percentage of molecules that was photoconverted to the HS state inferred from $\chi_M T$ values at 42, 25, and 42 K for C_6-**2**, C_{12}-**2**, and C_{18}-**2** is 80%, 54%, 50%, respectively.[22] The critical temperature of relaxation of the HS metastable state known as T^{LIESST} [5a] is 56 K (C_6-**2**),

(16) Brewer, G.; Luckett, C.; May, L.; Beatty, A. M.; Scheidt, W. R. *Inorg. Chim. Acta* **2004**, *357*, 2390−2396.

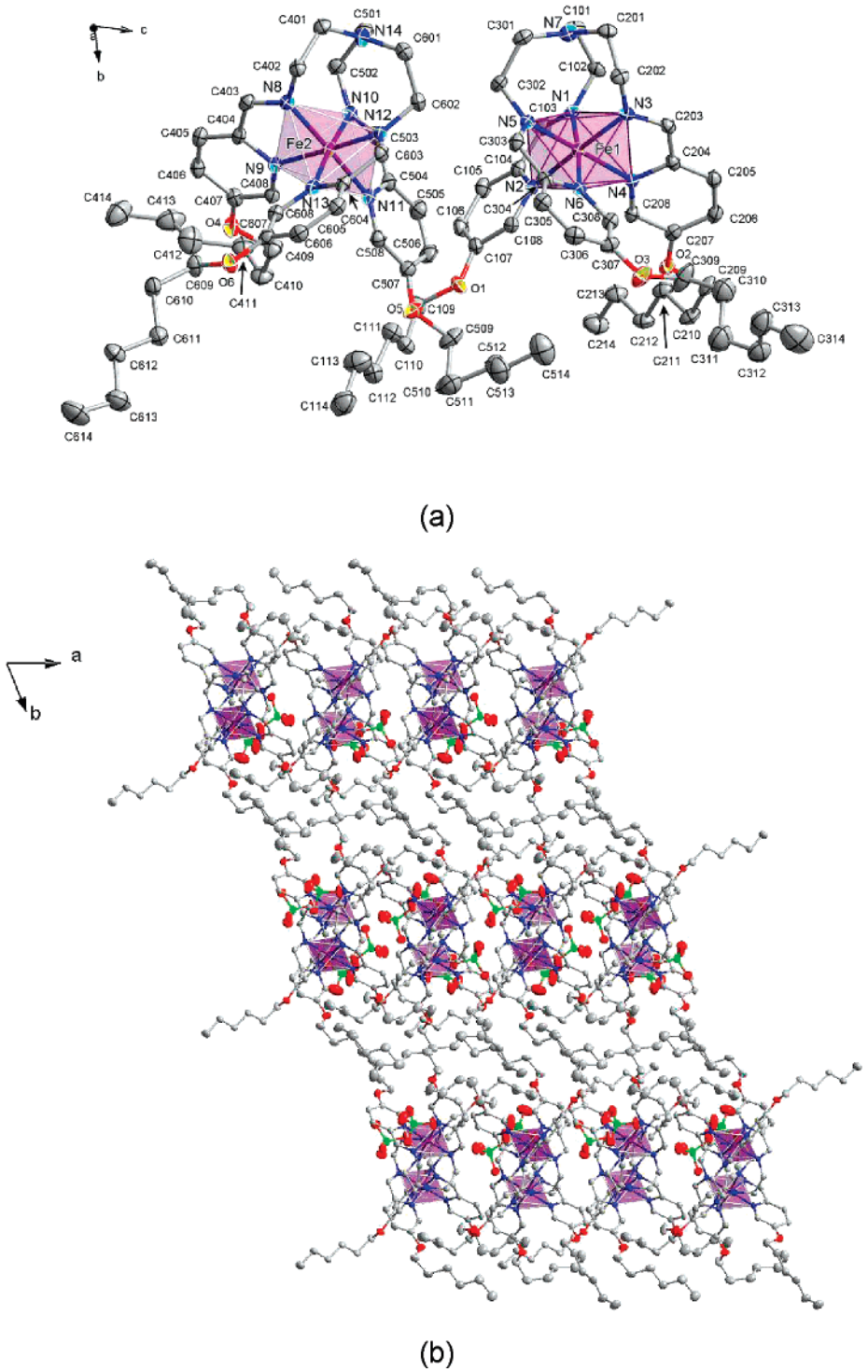

Figure 1. (a) Projection of the two independent cations of $[Fe(C_6\text{-trenH})]^{2+}$ with atom numbering scheme (150 K). (b) Projection of the molecular packing of C_6-**1** along the *c*-axis. Displacement ellipsoids are shown at 50% probability level. Hydrogen atoms and perchlorate anions are omitted for clarity.

48 K (C_{12}-**2**), and 56 K (C_{18}-**2**). XRD profiles of the complexes C_{18}-**1**, C_{12}-**2**, and C_{18}-**2** have been recorded at 300 and 410 K (SFigure 5). The X-ray diffraction patterns of the mesophase of these complexes gave a single sharp low angle (10) reflection and weak high-order reflection(s) all corresponding to the layer spacing. An additional diffuse reflection observed at larger angles refers to the average lateral spacing between alkyl chains. Upon Cr → S_A phase transition a shift of the low and high angle reflections to lower values with change of the intensity for the higher reflections and broadening of the alkyl reflection is observed. From the maxima of the reflections average interlayer distances *d* are obtained in both solid and liquid crystalline states (Table 1). On the basis of these findings for C_{18}-**1**, C_{12}-**2**, C_{18}-**2** at high temperature a smectic mesophase S_X has been identified with layered structures similar to C_6-**1** and C_6-**2**. DSC experiments performed at a rate of 10 K/min, in the warming and cooling modes, are shown for C_{18}-**1**, C_{12}-**2**, C_{18}-**2** in SFigure 4. Table 1 gathers the critical temperatures of melting, isotropi-

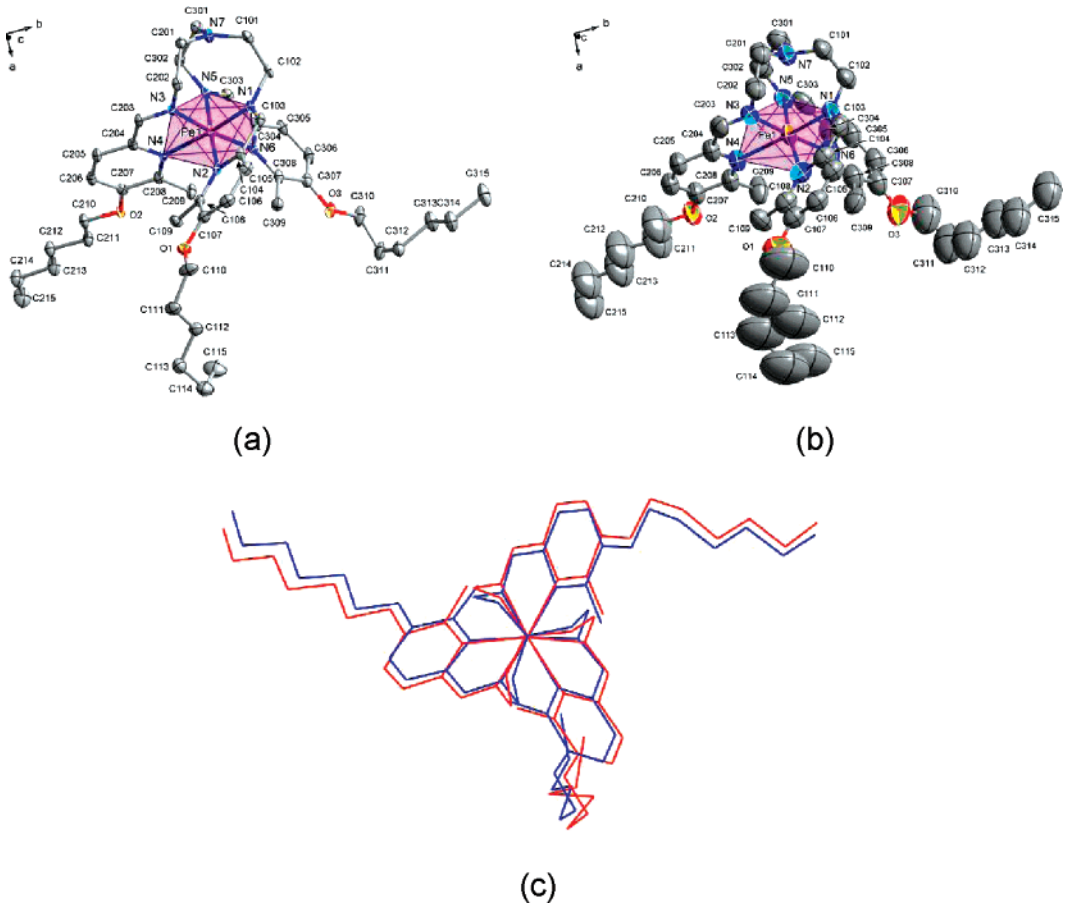

Figure 2. (a) Projection of the cations $[Fe(C_6\text{-trenMe})]^{2+}$ at 90 K and (b) at 298 K with atom numbering scheme. Hydrogen atoms and perchlorate anions are omitted for clarity. Displacement ellipsoids are shown at 50% probability level. (c) Projection along Fe···N7 axis of the minimized overlay of the cation $[Fe(C_6\text{-trenMe})]^{2+}$ in the LS state at 90 K (blue) and in the HS state at 298 K (red).

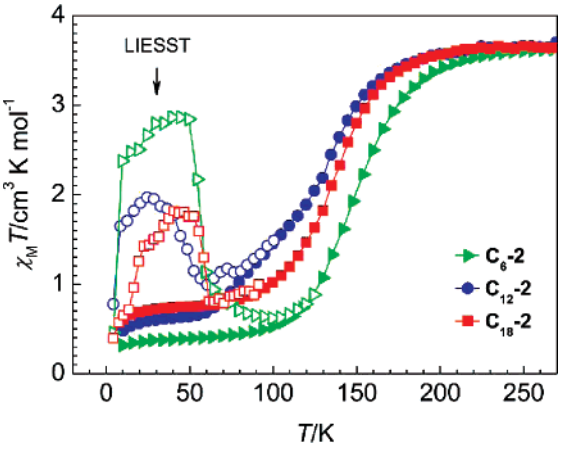

Figure 3. Magnetic properties in the form of $\chi_M T$ versus T for C_n-**2** ($n = 6, 12, 18$) and LIESST experiments[21] with irradiation at 4 K ($\lambda = 514$ nm, 25 mW cm^{-2}) and subsequently moving up in temperature (open symbols).

sation and decomposition deduced from differential scanning calorimetry (DSC), optical polarizing microscopy (OPM), and thermogravimetric analysis (TGA).

The lengthening of alkyl chains in C_n-**2** provokes a decrease of $T_{1/2}$, however, not in the linear way. In fact, compounds C_n-**2** are obtained at ambient temperature in HS form, and they adopt packing of molecular parts favoring bulkier HS polar heads. This could play a role in the shift of SCO in higher homologues C_{12}-**2** and C_{18}-**2** to lower temperature compared to the one observed in C_6-**2**. Packed long alkyl chains to some extent may prevent contraction of the cavity within the trifurcated ligand with an encapsulated iron(II) ion. The effect is rather weak causing the shift to lower temperature by ~15 K for C_{18}-**2**.

Magnetic and Mesomorphic Behavior of Compounds C_n-3 to C_n-5 (n = 16, 18, 20), C_{18}-6 to C_{18}-9. The compounds $[Fe(C_n\text{-trenH})](Cl)_2 \cdot 3.5H_2O$, $n = 16$ (C_{16}-**3**), 18 (C_{18}-**3**), 20 (C_{20}-**3**) and $[Fe(C_{18}\text{-tren})](F)_2 \cdot 3.5H_2O$ (C_{18}-**6**) show a very particular spin-state change, while $[Fe(C_{18}\text{-tren})](Br)_2 \cdot 3H_2O$ (C_{18}-**8**) and $[Fe(C_{18}\text{-tren})](I)_2$ (C_{18}-**9**) are in the LS state (10−400 K) and present mesomorphic behavior like that observed for the complexes C_{18}-**1**, C_{12}-**2**, and C_{18}-**2** (Table 1, SFigure 2−5). Figure 4a) illustrates the $\chi_M T$ versus T plots for C_{16}-**3**, a partial hydrate ($s = 0.5$) C_{16}-**4** and for the completely dehydrated complex C_{16}-**5** ($s = 0$) together with the corresponding Mössbauer spectra recorded at 80 K. Compound C_{16}-**3** is in the LS state at 300 K as confirmed by the $\chi_M T$ value of 0.02 cm^3 K mol^{-1} as well as by the Mössbauer spectrum. It is worth noting that the Mössbauer spectrum of C_{16}-**3** at 80 K shows two strongly overlapping doublets corresponding to two nonequivalent Fe(II) positions in the LS state (STable 3, SFigure 3). Upon heating $\chi_M T$ increases abruptly, attaining the value of 1.75 cm^3 K mol^{-1} at 400 K, where around 50% of the Fe(II) ions have converted to the HS state. TGA experiments have shown that dehydration takes place in the same temperature region where the spin-state change occurs (SFigure 1). Ad-

Table 1. Mass Spectroscopy Data, Thermal Transition and Mesomorphism, Interlayer Distances, Enthalpy, and Thermal Stability Determined by MS, OPM, DSC, and X-ray Diffraction for Compounds C_n-**1** to C_n-**9**

compound	MS[a], *m/z*	d^{Cr} [Å][c]	$d^{Sx,\ 410K}$ [Å]	d^{Cr} [Å][e]	thermal transitions [K][f]	$\Delta H^{Cr\rightarrow Sx}$ [kJ mol^{-1}][g]
C_6-**1**	868 $[M+ClO_4]^+$, 385 $[M]^{++}$	16.6 [d]				
C_{18}-**1**	1373 $[M+ClO_4]^+$, 637 $[M]^{++}$ [b]	29.1	31.05	29.1	Cr 370 S_X 473 d	49.6
C_6-**2**	910 $[M+ClO_4]^+$	17.4 (90 K), 17.9 (290 K) [d]				
C_{12}-**2**	1163 $[M+ClO_4]^+$	24.0	24.8	24.0	Cr 370 S_X 470 d	39.0
C_{18}-**2**	1415 $[M+ClO_4]^+$	29.6	31.3	29.5	Cr 373 S_X 470 d	54.9
C_{16}-**3**	1225 $[M+Cl]^+$	34.7	39.1	38.7	Cr 287 S_A 456 i(d)	28.1
C_{18}-**3**	1309 $[M+Cl]^+$, 637 $[M]^{++}$	36.0	42.3	40.1	Cr 301 S_A 463 i(d)	38.5
C_{20}-**3**	1393 $[M+Cl]^+$, 679 $[M]^{++}$	37.7	45.0	44.1	Cr 330 S_A 449 i(d)	63.8
C_{18}-**6**	1293 $[M+F]^+$ [b], 637 $[M]^{++}$	37.8	38.6	37.8	Cr 320 S_X 439 i(d)	53.5
C_{18}-**8**	1353 $[M+Br]^+$ [b], 637 $[M]^{++}$	35.8	39.1	39.7	Cr 325 S_X 451 i(d)	62.4
C_{18}-**9**	1401 $[M+I]^+$, 637 $[M]^{++}$	32.5	31.3	31.3	Cr 393 S_X 456 i(d)	65.7

[a] ESI or FD. [b] Trace. [c] Interlayer distance before first heating. [d] From the monocrystal X-ray data. [e] Interlayer distance after first heating. [f] Measured by DSC on the second heating scan. Isotropisation (decomposition) points are determined by OPM; decomposition confirmed by TGA. [g] DSC $\Delta H^{Cr\rightarrow Sx}$ data for the second heating scan.

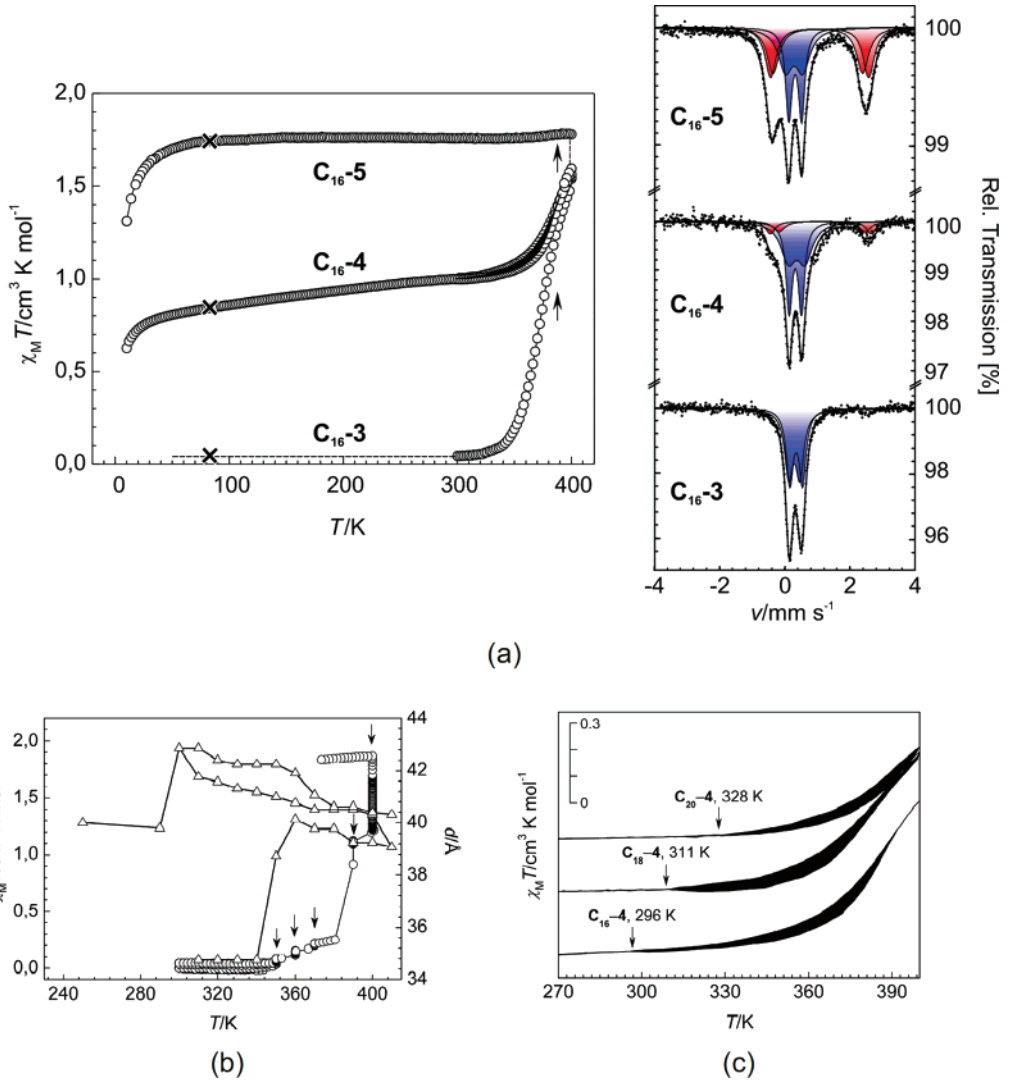

Figure 4. (a) $\chi_M T$ versus T for C_{16}-**3**, C_{16}-**4** and C_{16}-**5**: The symbol × denotes the temperature (80 K) at which the Mössbauer spectra (shown on the right) were recorded (HS doublet, red; LS doublet, blue). (b) Variation of the interlayer distance d with temperature (△) in C_{16}-**3** and C_{16}-**4** deduced from XRD profiles after following the sequence 310−410 to 230−410 K together with dehydration experiments in C_{16}-**3** monitored by temperature dependence of the magnetic susceptibility (○).[23] (c) $\chi_M T$ versus T for C_{16}-**4**, C_{18}-**4**, and C_{20}-**4** arrows indicate the temperatures at which heating and cooling curves diverge. The black areas indicate the hysteresis loops.

ditionally, DSC profiles, OPM analysis, and XRD patterns of C_{16}-**3** (SFigures 4, 5) show that the melting occurs at 340 K (first heating scan). At this point the following question emerges: does the solid↔liquid crystal phase transition during the first heating drive the spin transition in C_{16}-**3** or is it driven by the loss of water?

To answer this question we have performed dehydration experiments[23] in C_{16}-**3** monitoring the temperature dependence of the magnetic susceptibility (Figure 4b) and have recorded temperature-dependent XRD patterns following the sequence 310−410 to 230−410 K (SFigure 5). The sample was heated and subsequently cooled during several cycles between 280 (LS state) and 350 K. The $\chi_M T$ value after three cycles of melting↔solidification (287 K second heating scan) does not show any noticeable variation. In addition, the temperature variation of *d* derived from XRD patterns (Figure 4b) present an abrupt increase as a consequence of the melting between 340 and 350 K, but the increase in the $\chi_M T$ value begins at 360 K. Consequently, the hypothesis that the phase transition to the mesophase drives the spin-state change can be ruled out, at least in the present compound (C_{16}-**3**). On the contrary, it is clearly seen in the dehydration experiments that the magnetic susceptibility increases upon losing water, which matches with reported TGA data, and is completely accomplished at 400 K. For compound C_{16}-**3** 50% of the Fe(II) ions undergo spin-state change at $T_{1/2} = 375$ K induced by releasing water. Synergy between desolvation and spin-state change as observed in C_{16}-**3** has been reported in several cases.[1,13]

For the fully dehydrated material C_{16}-**5** the Mössbauer spectrum recorded at 80 K gives the following relative populations for the two inequivalent iron sites (1,2) in different spin states: For Fe(1) they are 25% (HS), 25%(LS); for Fe(2) they are 25% (HS), 25%(LS) (STable 3, SFigure 3). The $\chi_M T$ versus *T* plot for C_{16}-**5** agrees well with the Mössbauer spectrum and is characteristic of Fe(II) ions in the HS state (Figure 4a). The magnetic properties of a partially dehydrated C_{16}-**4** has also been investigated, which discloses interesting synergy between spin transition and change of the aggregate state of matter (solid↔liquid crystal). Figure 4a displays the $\chi_M T$ versus *T* plot for C_{16}-**4**. The partial dehydration of C_{16}-**3** was monitored by recording $\chi_M T$ versus *T* during two cycles of warming−cooling following the sequence 300−400 to 10−400 K and proved by TGA analysis that C_{16}-**4** was left (SFigure 1). For C_{16}-**4**, the $\chi_M T$ versus *T* between 400 and 296 K presents a variation accompanied by a narrow hysteresis. Below 296 K $\chi_M T$ remains almost constant until 10 K, where it sharply decreases as a consequence of the zero-field splitting of the Fe(II) ions remaining in the HS state (18%, STable 3). The thermally induced spin transition in C_{16}-**4** starts right after the onset of the first-order phase transition (Cr↔S_A). Since the spin transition is blocked below the temperature at which the compound solidifies, one can conclude that the melting process drives the spin transition in this compound. The fact that the spin transition inside the SA mesophase is accompanied by hysteresis is not surprising since in the present state of the material the spin transition is not expected to follow a Boltzmann distribution of spin states as observed in the liquid state.[1a] Indeed, spin transition accompanied by hysteresis has been observed earlier in the compounds $[Fe(C_n\text{-trz})_3](4\text{-}MeC_6H_4SO_3)_2$ in the region of existence of the D_{hd} mesophase.[13] One remarkable fact is that the compounds C_{18}-**3** and C_{20}-**3** behave similarly as C_{16}-**3**. The results of physical studies of these materials are presented in SFigures 1−5. For a comparative analysis Figure 4c shows the $\chi_M T$ versus *T* plots for C_n-**4** ($n = 16, 18, 20$). It is worth mentioning that the spin-transition temperature is determined by the melting temperature which is higher for the derivatives with longer alkyl chains. For compound C_{18}-**6** no partial hydrate can be obtained like in the case of C_n-**3**, but the full dehydration provokes the spin-state change of near 50% of the Fe(II) ions (SFigures 1−5). The compounds C_n-**3** and C_{18}-**6** are dark purple in the LS state and become light purple-brown when 50% of the Fe(II) atoms are in the HS state.

Conclusion

In view of the experimental results the answer to the question posed in the title is yes, for some type of spin crossover metallomesogens.

Compounds C_{18}-**1**, C_{18}-**8**, and C_{18}-**9** do not present SCO behavior in the region of temperatures investigated (10−400 K) but exhibit mesomorphic behavior. Compounds C_{12}-**2** and C_{18}-**2** can be classified as type iii in view of the different phase transitions occurring in these materials taking place in very different temperature regions. Therefore, any interplay/synergy between different physical phenomena, spin transition, and change of aggregate state of matter (solid↔liquid crystal), can be anticipated. On the other hand, the compounds C_n-**3** and C_{18}-**6** (type ii) are new examples of materials in which the two phase transitions coexist in the same temperature region but are not coupled. These very interesting materials present change of aggregate state of matter and spin-state change upon dehydration in a narrow temperature interval. The compounds C_n-**4** represent the first examples of systems in which the solid↔liquid crystal transition drives the spin-state transition.

As mentioned in the introduction, complete control of the variables that affect the spin-crossover behavior in solid state is a rather difficult task to accomplish, since it depends essentially on the nature of the ligands, the non-coordinating anions, the solvent molecules, and the crystal packing.[1] This is particularly accentuated for monomeric complexes as the communication between the SCO centers is achieved exclusively through intermolecular interactions, such as hydrogen bonding or $\pi-\pi$ interactions between aromatic ligands, anions, and solvent molecules. In polymeric compounds, partial or total substitution of these intermolecular interactions by covalent linkage of the metal centers leads to a more predictable control of the spin-transition behavior.

The general observation in $[Fe(C_n\text{-trenH})](A)_2 \cdot sH_2O$ A = F^-, Cl^-, Br^- and I^- metallomesogens is that the spin state depends mainly on the degree of hydration of the compound and not on the state of the matter, solid or liquid. In fact, only for the particular cases of derivatives C_n-**4** do the structural changes associated to the Cr↔LC phase transition drive the spin-state transition. Seemingly, the effect of the different electronegativity of halogenated counterions is less important in determining the crystal field strength at the iron(II) center. In contrast, no solvates were isolated in the case of perchlorate derivatives $[Fe(C_n\text{-trenH})](ClO_4)_2$,where the LS state is the preferred spin state. Introduction of the alkyl group in the ligand C_n-trenR decreases the ligand field strength at the Fe(II) center leading to a spin crossover behavior in $[Fe(C_n\text{-trenMe})](ClO_4)_2$.

In some instances correlations between anion size and transition temperature have been proposed[1,17] but the general validity has not been established. The effects of the anion and solvation are, however, not always consistent from one system to another and are not readily predictable. Replacement of the anion or solvent molecule is expected to modify the lattice

phonon distribution resulting from different crystal packing geometry or strength of the intermolecular forces. In addition, changes in the chemical composition of the lattice could impose different degrees of "chemical pressure" (also known as "image pressure") on the spin transition centers and thereby influence the transition temperature. Hydrogen bonding can be a major influence on both the transition temperature (in part at least by affecting the ligand field strength) and the nature of the transition, providing the structural links for communication between the SCO centers. Thus the extent to which an anion or solvate molecule can hydrogen bond with the SCO center will likely influence the nature of the transition.[1]

It has been proposed that hydration will generally result in a stabilization of the LS state, through hydrogen bonding of the water molecule with the ligand[1]. This indeed seems to be the case for most hydrates, but in a cationic SCO system where the ligand is hydrogen bonded to the associated anion only and this in turn is bonded to the water molecule, the effect can be the reverse, that is, loss of water can also result in stabilization of the LS state. Whatever the rationale for the effects, it is clear that variation in the nature of the anion or the solvation is a very readily accessible, if not entirely predictable, means of potentially modulating the transition temperature or the nature of the transition.[1]

In this study we have shown that synchronization of spin state and liquid crystal transitions is achieved by the search for a parent SCO system suitable, after attaching the liquid crystal moiety, to possess LS state or SCO properties at the temperature where the solid↔liquid crystal is foreseen (275−400 K). We have demonstrated that the required criteria could be satisfied by modifying the original SCO system $\{Fe[tren(Py)_3]\}(ClO_4)_2$.[16]

Experimental Section

Physical Measurements. Variable-temperature magnetic susceptibility measurements of samples of C_n-**1** to C_n-**9** (20−30 mg) were recorded with a Quantum Design MPMS2SQUID susceptometer equipped with a 7 T magnet, operating at 1 T and at temperatures from 1.8 to 400 K. The susceptometer was calibrated with $(NH_4)_2Mn(SO_4)_2{\cdot}12H_2O$. Experimental susceptibilities were corrected for diamagnetism of the constituent atoms by the use of Pascal's constants. Mössbauer spectra were recorded in transmission geometry with a ^{57}Co/Rh source kept at room temperature and a conventional spectrometer operating in the constant-acceleration mode. The samples were sealed in Plexiglass sample holders and mounted in a nitrogen-bath cryostat. The Recoil 1.03a Mössbauer Analysis Software (Dr. E. Lagarec; http://www.isapps.ca/recoil/) was used to fit the experimental spectra. DSC measurements were performed on a Mettler model DSC 822e calibrated with metallic indium and zinc. DSC profiles were recorded at the rate of 10 K/min and analyzed with Netzsch Proteus software (NETZSCH-Geraetebau GMBH, http://www.e-thermal.com/proteus.htm). An overall accuracy of 0.2 K in the temperature and 2% in the heat flow has been estimated. X-ray powder diffraction measurements were carried out with a Seifert TT3300 diffractometer (monochromatic Cu Kα radiation). The temperatures and textures of phase transitions were determined with a polarization microscope, equipped with a hot stage and with temperature control of better than ± 0.5 K. IR spectra were recorded at 298 K using a Brooker Tensor 27 spectrometer in the range of 400−4000 cm^{-1}. Elemental analyses were done on a Vario EL Mikro Elementaranalysator. ^{1}H NMR spectroscopic measurements were done on an Advance DRX Bruker 400 MHz Spectrometer. TGA measurements were performed on a Mettler Toledo TGA/SDTA 851, in the 300−680 K temperature range in nitrogen atmosphere with a rate of 10 K/min. Mass spectra were recorded on Finnegan MAT 95 (Field Desorption, FD) and Micromass Q-TOF2 (Electro Spray Ionization, ESI).

X-ray Structure Determination. The data were collected using an Oxford Diffraction KM4 κ diffractometer with a Sapphire3 CCD detector and graphite-monochromated Mo Kα radiation (0.71073 Å). The crystals were mounted on a quartz glass capillary and cooled by a cold, dry nitrogen gas stream (Oxford Cryosystems equipment). The temperature stability was ± 0.1 K. Accurate cell parameters were determined and refined using the program CrysAlis CCD.[18] For the integration of the collected data the program CrysAlis RED was used.[19] The structure was solved using the direct method with SHELXS-97 software, and the solution was refined with SHELXL-97.[20] All non-hydrogen atoms were refined with anisotropic temperature factors. CCDC 658238−658240 contains the supplementary crystallographic data for compounds C_6-**1** and C_6-**2**. This data can be obtained free of charge from The Cambridge Crystallographic Data Centre via www.ccdc.cam.ac.uk/data_request/cif.

Synthesis of Materials. Starting reagents and solvents were obtained commercially from Aldrich or Acros and used as received. The synthesis of the precursors for the ligands C_n-trenH and C_n-trenMe is described in the Supporting Information.

General Synthetic Procedure for Compounds C_n-N (n = 6, 12, 16, 18, 20; N = 1, 2, 3, 6, 8, 9). General Procedure for Alkoxy-Substituted Systems. A batch of an alkylated picolinaldehyde and a stoichometric amount of tris(2-aminoethyl)amine (tren) were dissolved in ethanol, the calculated amount of iron(II) salt was added which was immediately accompanied by intensive coloration. The mixture was stirred for 15 min and then transferred into a refrigerator and left at 4 °C over night. The crystalline precipitate was filtered off, washed with ethanol, and dried in vacuo.

C_6-**1.** tren (0.05 g, 0.34 mmol), excess of crude 5-(hexyloxy)-picolinaldehyde, $Fe(ClO_4)_2{\cdot}xH_2O$ (0.087 g, 0.34 mmol). FT-IR (KBr; cm^{-1}): 2928, 2851 ν(C−H), 1616 ν(C═N), 1090, 622 ν(Cl−O). Anal. Calcd for $C_{42}H_{63}Cl_2FeN_7O_{11}$: C, 52.07; H, 6.55; N, 10.12. Found: C, 51.98; H, 6.53; N, 10.09.

C_{18}-**1.** tren (0.05 g, 0.34 mmol), 5-(octadecyloxy)picolinaldehyde (0.38 g, 1.02 mmol), $Fe(ClO_4)_2{\cdot}xH_2O$ (0.087 g, 0.34 mmol). FT-IR (KBr; cm^{-1}): 2918, 2850 ν(C−H), 1616 ν(C═N), 1093, 622 ν(Cl−O). Anal. Calcd for $C_{78}H_{135}Cl_2FeN_7O_{11}$: C, 63.57; H, 9.23; N, 6.65. Found: C, 63.45; H, 8.82; N, 6.46.

C_6-**2.** tren (0.05 g, 0.34 mmol), excess of crude 6-methyl-5-(hexyloxy)picolinaldehyde, $Fe(ClO_4)_2{\cdot}xH_2O$ (0.087 g, 0.34 mmol). FT-

(17) (a) Garcia, Y.; van Koningsbruggen, P. J.; Lapouyade, R.; Rabardel, L.; Kahn, O.; Wieczorek, M.; Bronisz, R.; Ciunik, Z.; Rudolf, M. F. *C. R. Acad. Sci., Ser. II C* **1998**, *1*, 523−532. (b) Lavrenova, L. G.; Ikorski, V. N.; Varnek, V. A.; Oglezhneva, I. M.; Larionov, S. V. *Koord. Khim.* **1986**, *12*, 207−215. (c) Varnek, V. A.; Lavrenova, L. G. *J. Struct. Chem.* **1995**, *36*, 104−111. (d) Lemercier, G.; Verelst, M.; Bousseksou, A.; Varret, F.; Tuchagues, J.-P. In *Magnetism: a supramolecular function*; Kahn, O., Ed.; NATO Advanced Study Institute Series; Kluwer Academic Publishers: Dordrecht, The Netherlands, 1996; Vol. C484, p 335.

(18) *CrysAlis CCD*, version 1.171.29; Oxford Diffraction Ltd: Poland, 2006; Wrocław.

(19) *CrysAlis RED*, version 1.171.29; Oxford Diffraction Ltd: Poland, 2006; Wrocław.

(20) Sheldrick, G. M. *SHELXS97/SHELXL97*; University of Göttingen: Göttingen, Germany, 1997.

(21) The sample was irradiated at 4 K (LS state) with light of λ = 514 nm (25 mW cm^{-2}) until saturation of the magnetic moment was reached. Then irradiation was switched off and $\chi_M T$ versus T was recorded in the warming mode at a rate of 2 K/min up to 300 K. At temperatures greater than 70 K, $\chi_M T$ increases following the spin-transition curve observed for each compound.

(22) The sharp rise of $\chi_M T$ with increasing temperature below the maximum conversion is due to the well-known zero-field splitting effect.

(23) The hydrated samples were placed in open containers in the SQUID sample holder and their magnetism measured. The first part of the experiment comprised several cycles of heating−cooling from 280 until 350 K (empty squares). Then, the samples were left for 2 h at the reported temperatures (indicated by arrows) and the magnetic moment was measured (open circles). Dehydration taking place under these conditions is confirmed by the thermogravimetric analysis (SFigure 1).

IR (KBr; cm^{-1}): 2929, 2855 ν(C−H), 1651 ν(C═N), 1080, 622 ν(Cl−O). Anal. Calcd for $C_{45}H_{69}Cl_2FeN_7O_{11}$: C, 53.47; H, 6.88; N, 9.70. Found: C, 53.72; H, 6.53; N, 9.82.

C_{12}-**2.** tren (0.05 g, 0.34 mmol), excess of crude 6-methyl-5-(dodecyloxy)picolinaldehyde, $Fe(ClO_4)_2 \cdot xH_2O$ (0.087 g, 0.34 mmol). FT-IR (KBr; cm^{-1}): 2914, 2851 ν(C−H), 1651 ν(C═N), 1088, 622 ν(Cl−O). Anal. Calcd for $C_{45}H_{69}Cl_2FeN_7O_{11}$: C, 60.73; H, 8.57; N, 7.51. Found C, 59.79; H, 8.37; N, 7.74.

C_{18}-**2.** tren (0.05 g, 0.34 mmol), 6-methyl-5-(octadecyloxy)picolinaldehyde (0.40 g, 1.02 mmol), $Fe(ClO_4)_2 \cdot xH_2O$ (0.087 g, 0.34 mmol). FT-IR (KBr; cm^{-1}) 2919, 2850 ν(CH), 1650 ν(C═N), 1088, 622 ν-(Cl−O). Anal. Calcd for $C_{78}H_{135}Cl_2FeN_7O_{11}$: C, 63.57; H, 9.23; N, 6.65. Found: C, 63.73; H, 9.27; N, 6.66.

C_{16}-**3.** tren (0.05 g, 0.34 mmol), 5-(hexadecyloxy)picolinaldehyde (0.35 g, 1.02 mmol), $FeCl_2 \cdot 4H_2O$ (0.07 g, 0.34 mmol). FT-IR (KBr; cm^{-1}): 3400br ν(O−H), 2917, 2850 ν(C−H), 1616 ν(C═N). Anal. Calcd for $C_{72}H_{130}Cl_2FeN_7O_{6.5}$: C, 65.29; H, 9.89; N, 7.40. Found: C, 65.63; H, 9.81; N, 7.31.

C_{18}-**3.** tren (0.05 g, 0.34 mmol), 5-(octadecyloxy)picolinaldehyde (0.38 g, 1.02 mmol), $FeCl_2 \cdot 4H_2O$ (0.07 g, 0.34 mmol). FT-IR (KBr; cm^{-1}): 3400br ν(O−H), 2918, 2850 ν(C−H), 1616 ν(C═N). Anal. Calcd for $C_{78}H_{142}Cl_2FeN_7O_{6.5}$: C, 66.50; H, 10.16; N, 6.96. Found: C, 66.74; H, 10.47; N, 6.69.

C_{20}-**3.** tren (0.05 g, 0.34 mmol), 5-(icosyloxy)picolinaldehyde (0.41 g, 1.02 mmol), $FeCl_2 \cdot 4H_2O$ (0.07 g, 0.34 mmol). FT-IR (KBr; cm^{-1}): 3400br ν(O−H), 2917, 2850 ν(C−H), 1616 ν(C═N). Anal. Calcd for $C_{84}H_{154}Cl_2FeN_7O_{6.5}$: C, 67.58; H, 10.40; N, 6.57. Found: C, 67.83; H, 10.12; N, 6.47.

C_{18}-**6.** tren (0.05 g, 0.34 mmol), 5-(octadecyloxy)picolinaldehyde (0.38 g, 1.02 mmol), $FeBr_2$ (0.073 g, 0.34 mmol), TlF in $EtOH/H_2O$ (0.15 g, 0.68 mmol). After mixing of components white precipitate of TlBr was filtered off, the solution was evaporated, and the remainder was recrystallized from hot EtOH. FT-IR (KBr; cm^{-1}): 3400br ν(O−H), 2917, 2850 ν(C−H), 1613 ν(C═N). Anal. Calcd for $C_{81}H_{148}F_2FeN_7O_{6.5}$: C, 68.09; H, 10.40; N, 7.13. Found: C, 68.32; H, 10.42; N, 6.54.

C_{18}-**8.** tren (0.05 g, 0.34 mmol), 5-(octadecyloxy)picolinaldehyde (0.38 g, 1.02 mmol), $FeBr_2$ (0.073 g, 0.34 mmol). FT-IR (KBr; cm^{-1}): 3400br ν(O−H), 2917, 2850 ν(C−H), 1616 ν(C═N). Anal. Calcd for $C_{78}H_{141}Br_2FeN_7O_6$: C, 62.55; H, 9.56; N, 6.55. Found: C, 62.15; H, 9.33; N, 6.43.

C_{18}-**9.** To $MeOH/CHCl_3$ (4:1) medium, tren (0.05 g, 0.34 mmol), 5-(octadecyloxy)picolinaldehyde (0.38 g, 1.02 mmol), $Fe(ClO_4)_2 \cdot xH_2O$ (0.087 g, 0.34 mmol), KI (0.11 g, 0.68 mmol) were added. After the mixing of components the white precipitate of $KClO_4$ was filtered off, the solution was evaporated, and the remainder was recrystallized from hot EtOH. FT-IR (KBr; cm^{-1}): 2917, 2850 ν(C−H), 1613 ν(C═N). Anal. Calcd for $C_{78}H_{135}I_2N_7O_3$: C, 61.29; H, 8.90; N, 6.41. Found: C, 61.83; H, 8.84; N, 6.26.

Acknowledgment. We acknowledge the financial help from the Deutsche Forschungsgemeinschaft (Priority Program 1137 "Molecular Magnetism"), the Fonds der Chemischen Industrie. A.B.G. thanks the Spanish MEC for a Ramon y Cajal research contract, for the project CTQ2004-03456-BQU, and the Alexander von Humboldt Foundation for work−visiting fellowships. Y.G. acknowledges the financial support from the DLR/BMBF project RUS 05/003 and RFBR Grant No. 03-03-32571. We also thank Ms. E. Muth and Ms. P. Räder of the Max-Planck-Institute for Polymer Research, Mainz, for their help in performing TGA and DSC measurements and Dr. Gutmann and Mr. M. Bach for help in performing temperature-dependent XRD measurements.

Supporting Information Available: Synthesis of the precursors for the ligands C_n-trenH and C_n-trenMe, scheme of synthetic procedure for compounds C_n-**N** (n = 6, 12, 16, 18, 20; N = **1**, **2**, **3**, **6**, **8**, **9**). TGA analysis of materials C_n-**3**, C_{18}-**6**, C_{18}-**8**, and C_{18}-**9**. Magnetic properties of compounds C_n-**1**, C_n-**3** to C_n-**5** (n = 18, 20), C_{18}-**6**, C_{18}-**8**, and C_{18}-**9** in the form of $\chi_M T$ versus T. Mössbauer spectra of compounds C_n-**1**, C_n-**2**, C_n-**3**, to C_n-**5** (n = 18 20), C_{18}-**6**, C_{18}-**7**, C_{18}-**8**, and C_{18}-**9**, at different temperatures. Mössbauer parameters for C_n-**1**, C_n-**2**, C_n-**3**, to C_n-**5** (n = 16, 18, 20), C_{18}-**6**, C_{18}-**7**, C_{18}-**8**, and C_{18}-**9**. DSC measurements for C_{18}-**1**, C_{12}-**2**, C_{18}-**2**, C_n-**3** to C_n-**5** (n = 16, 18, 20), C_{18}-**6**, C_{18}-**7**, C_{18}-**8**, and C_{18}-**9** in the heating and cooling mode performed at the rate of 10 K/min. XRD patterns for C_{18}-**1**, C_{12}-**2**, C_{18}-**2**, C_n-**3** to C_n-**5** (n = 16, 18, 20), C_{18}-**6**, C_{18}-**7**, C_{18}-**8**, and C_{18}-**9** recorded at different temperatures. Projection of the molecular packing of C_6-**2** along c-axis at 90 K.

JA077265Z